SUPPLEMENTARY INFORMATION

Microecology in vitro model replicates the human skin microbiome interactions

Pan Wang[1#], Huijuan Li[1#], Xingjiang Zhang[1], Xiaoxun Wang[1], Wenwen Sun[1], Xiaoya Zhang[1], Baiyi Chi[1], Yuyo Go[2], Xi Hui Felicia Chan[3], Jianxin Wu[1#]* & Qing Huang[1]*

[1]Skin Health and Cosmetic Development & Evaluation Laboratory, China Pharmaceutical University, Nanjing 211198 Jiangsu, China.

[2]Department of Engineering Science, University of Oxford, Parks Road, Oxford, UK, OX1 3PJ

[3]Department of Medicine, Waikato hospital, 183 Pembroke Street, Hamilton 3204, New Zealand

[#]These authors contributed equally: Pan Wang, Huijuan Li, Jianxin Wu

*Correspondence: wujianxin@cpu.edu.cn; huangqingcpu@163.com

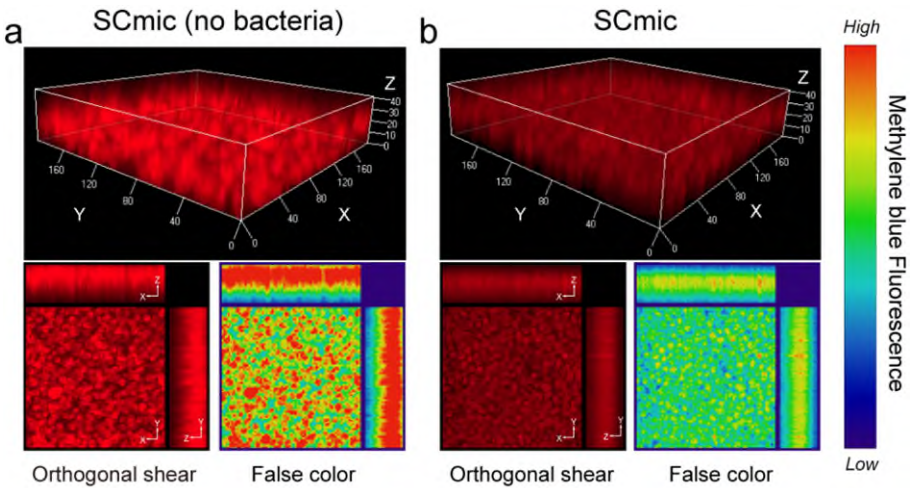

Supplementary Fig. 1 Formation of oxygen gradients in SCmic. **a** Fluorescence imaging of SCmic model without bacteria culture. **b** Fluorescence imaging of SCmic model after 24 hours of bacteria culture. Methylene blue produces high fluorescence intensity at high oxygen levels. Methylene blue exhibits high fluorescence intensity in regions with elevated oxygen levels. The image shown is representative of n=3 independent replicates of experiments with similar results.

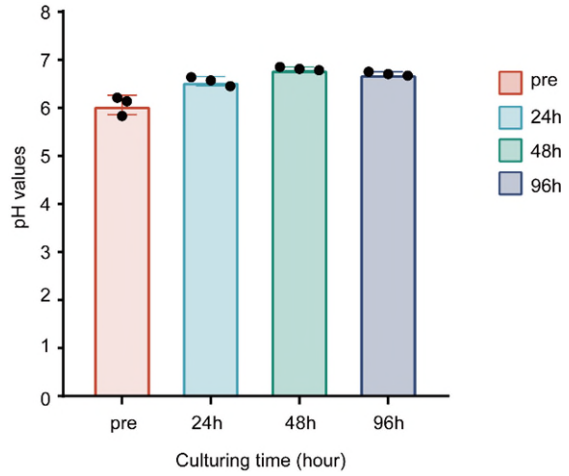

Supplementary Fig. 2 The pH values of the surface of the SCmic model was detected by a skin pH meter at each time points before inoculation with the Hcm community and after incubation. Error bars represent mean ± SD for three biological independent replicates. Source data are provided as a Source Data file.

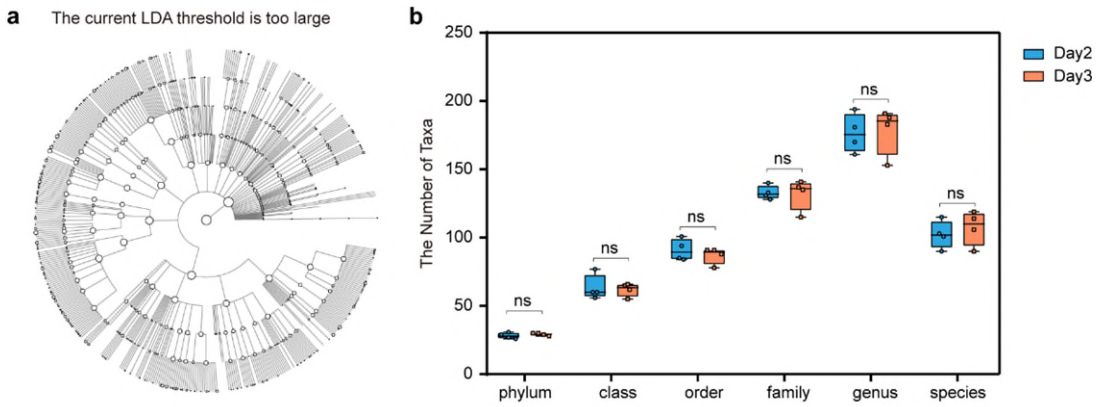

Supplementary Fig. 3 No significant differences between the two groups from phylum to family to genus. **a** The taxonomic clade shows the taxonomic hierarchical relationships of the main taxa in the day2 and day3 community, from phylum to genus (from inner circle to outer circle). Differences were identified by linear discriminant analysis (LDA) effect size analysis (LEfSe, LDA score >2.5), hollow nodes represent taxa that do not differ significantly between groups. **b** The number of taxa that differed between the two groups at the phylum, family, and genus levels was assessed using a one-way ANOVA. No statistically significant differences ($^{ns}p > 0.05$) were observed. The boxplots denote the median with a quartile range (25–75%), and the length of whiskers represents 1.5× the IQR. n=4 technical replicates. Source data are provided as a Source Data file.

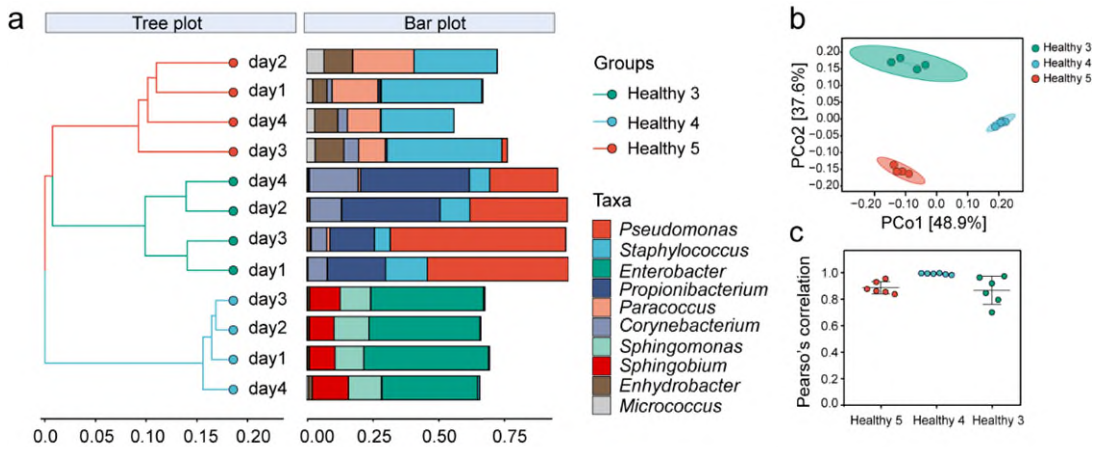

Supplementary Fig. 4 The skin microbiome in healthy individuals remains stable over short periods. **a** UPGMA phylogenetic tree constructed based on weighted Unifrac distances; bar plot shows top 10 genera abundance. **b** Principal Coordinate Analysis (PCoA) plots (based on weighted Unifrac) analyzing changes in microbiota over four days on the skin. **c** Pearson's correlation coefficient (r) between the skin microbiota on each day over four days and the average community of day one. The boxplots denote the median with a quartile range (25–75%), and the length of whiskers represents 1.5× the IQR, n=4 biologically independent microbiomes. Source data are provided as a Source Data file.

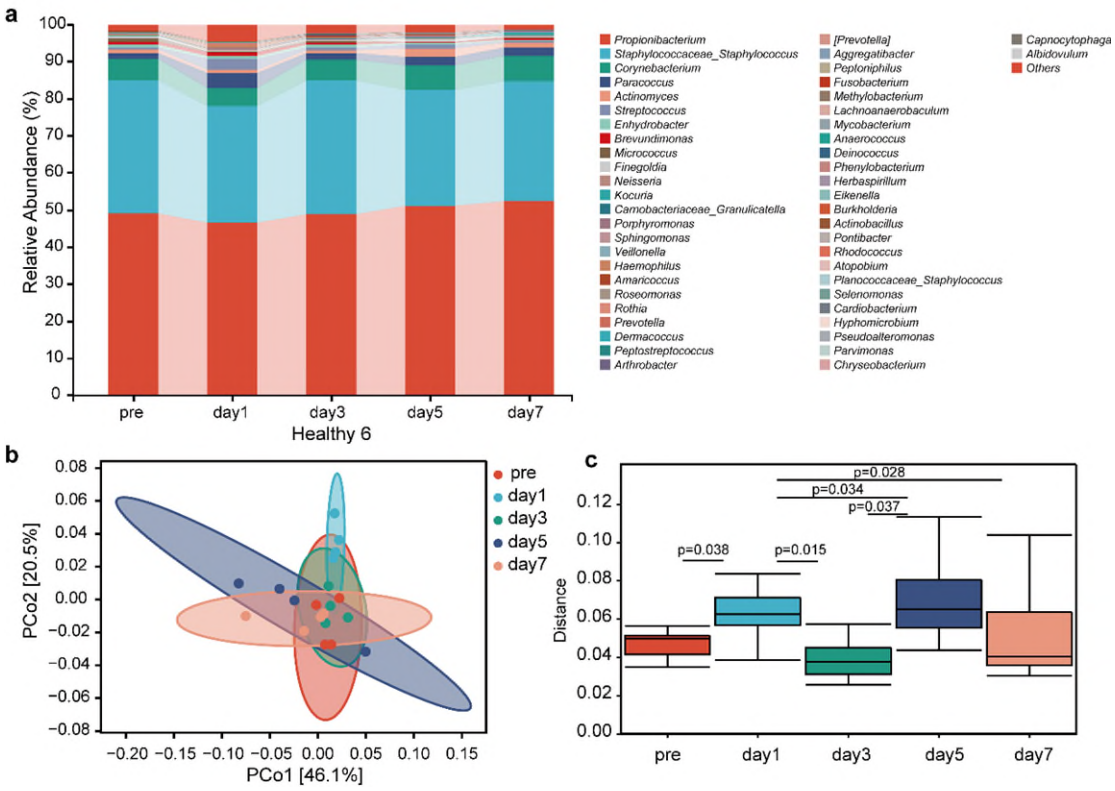

Supplementary Fig. 5 The skin microbiome remains stable on the model over time. **a** The composition bar plot shows the distribution of microbiome genera-level biomass in the model over 0-7 days of culture, n=4 biologically independent microbiomes. **b** Principal coordinate analysis (PCoA) plot (based on weighted Unifrac) of normal microbiota cultured for 0-7 days. **c** Analysis of similarities (Anosim) based on weighted Unifrac distance matrix shows differences between the microbiota of normal for pre, day1, day3, day5 and day7. The boxplots denote the median with a quartile range (25–75%), and the length of whiskers represents 1.5× the IQR, n=4 biologically independent microbiomes. Source data are provided as a Source Data file.

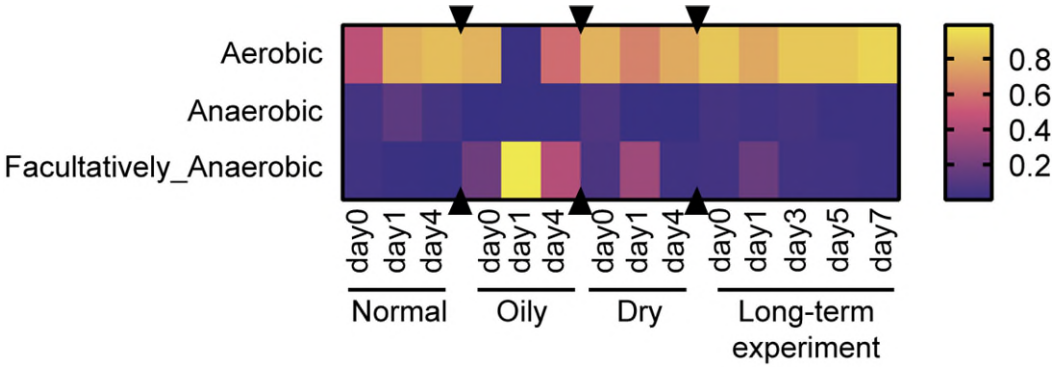

Supplementary Fig. 6 BugBase prediction of oxygen utilization for microbiota across all experiments. Source data are provided as a Source Data file.

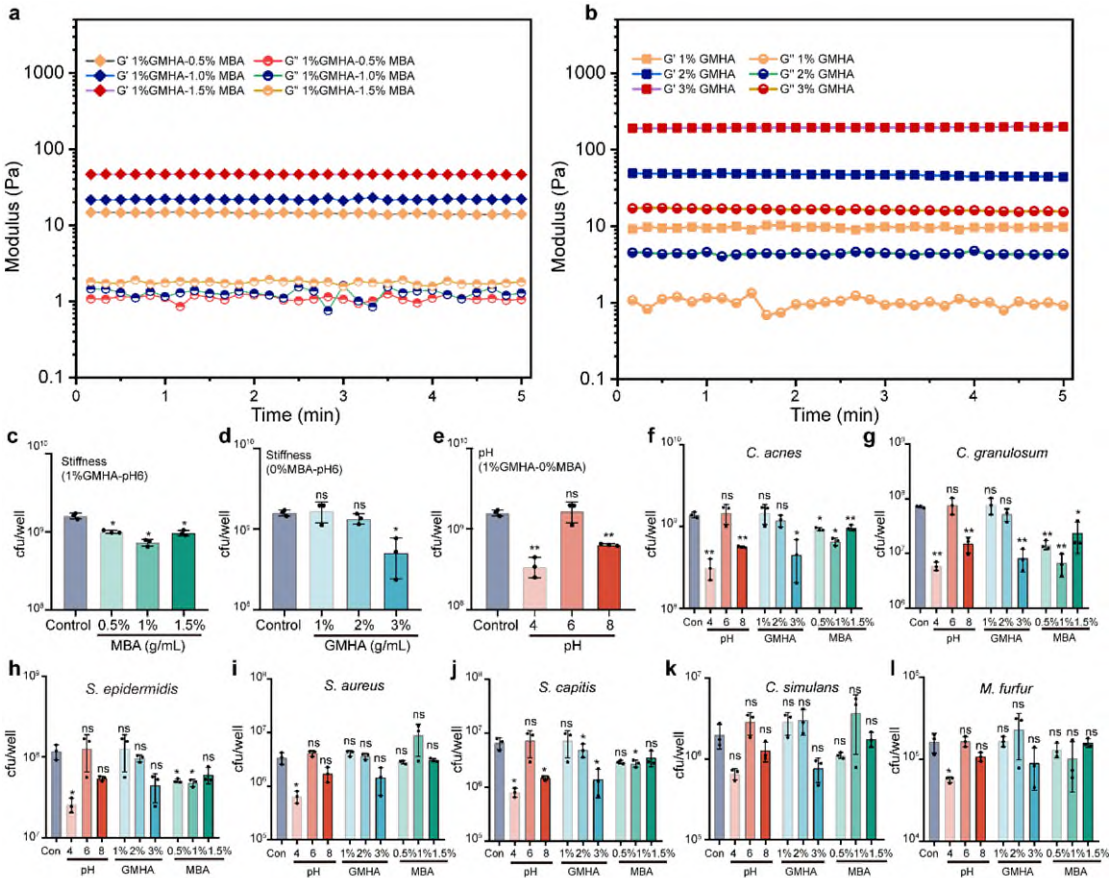

Supplementary Fig. 7 Influence of gel characteristics on microbiota in the SCmic model. **a** Energy storage modulus (G') and loss modulus (G'') of hydrogels with varying N, N'-methylene diacrylamide (MBA) crosslinker concentrations. **b** Energy storage modulus (G') and loss modulus (G'') of hydrogels with varying GMHA concentrations. **c** Effect of gel stiffness on total microbiota counts with 1% GMHA and varying MBA concentrations from 0.5-1.5%. **d** Effect of gel stiffness on total microbiota counts with varying GMHA concentrations from 1-3%. **e** Effect of gel on total microbiota under different pH conditions. **f-l** Effect of different pH values and gel stiffness on seven bacterial species in the microbiota: *C. acnes*, *C. granulosum*, *S. epidermidis*, *S. aureus*, *S. capitis*, *C. simulans*, and *M. furfur*. Statistical analyses were determined by two-tailed Student's t-test, $^{ns}P > 0.05$, $^{*}P < 0.05$, $^{**}P < 0.01$ vs control, Error bars represent mean ± SD for three biological independent replicates. Control: Hcm microbiota pre-culture. All experimental groups: Hcm microbiota were cultured on the model for 3 days at 32°C and 75%RH. Source data are provided as a Source Data file.

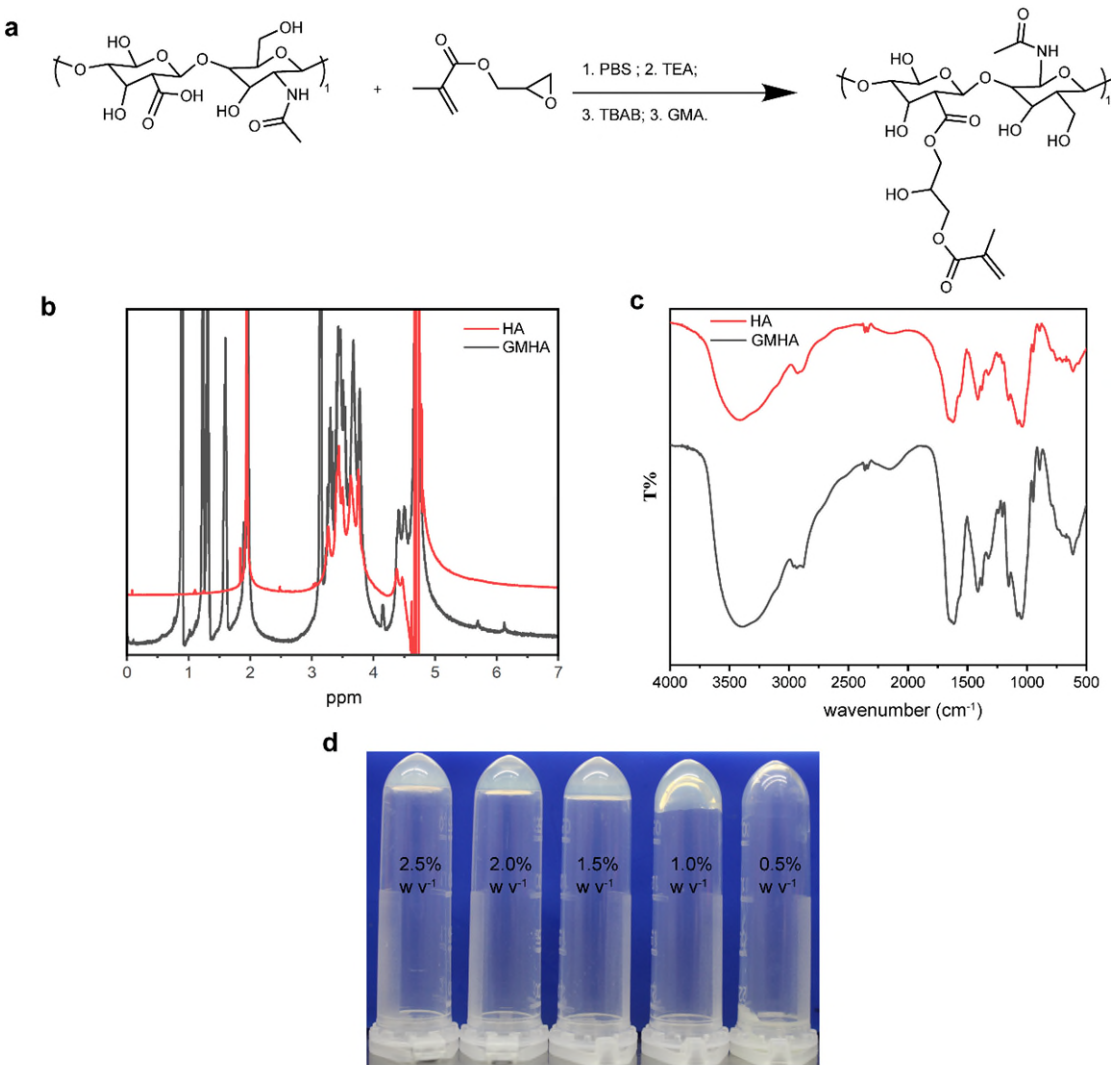

Supplementary Fig. 8 Characterization of GMHA synthesis and hydrogel formation. **a** Schematics of the chemical reactions of GMHA. PBS: phosphate buffer; GMA: glycidyl methacrylate. Triethylamine (TEA): Base condition; Tetrabutyl ammonium bromide (TBAB): As phase transfer catalyst. **b** ^{1}H-NMR spectrum confirming the successful grafting of glycidyl methacrylate (GM) onto hyaluronic acid (HA). Characteristic methacrylate peaks appear at 5.6 and 6.1 ppm, while the HA methyl peak is observed at 1.9 ppm. The degree of methacrylation was determined to be 26% based on peak integration. **c** FTIR spectrum of GMHA showing a distinct absorption band at 943 cm^{-1}, corresponding to the C=C double bond of the methacrylate group, confirming

successful GM grafting. **d** GMHA gel solution (0.5%-2.5% w v^{-1}) after 60 s of UV treatment, forming a stable crosslinked hydrogel at a minimum GMHA concentration of 1% (w v^{-1}) in the presence of 0.3% (w v^{-1}) lithium phenyl-2,4,6-trimethylbenzoylphosphinate (LAP).

Supplementary table 1

Some skin bacteria encoding the nicotinamidase PncA homologous protein, retrieved from NCBI search.

Protein ID	GI	Annotation	Species	Length
BDE67323.1	GI:2188772654	nicotinamidase	*Cutibacterium acnes*	193 AA
BDQ42155.1	GI:2438332621	nicotinamidase	*Cutibacterium acnes*	193 AA
BCB13046.1	GI:1820242239	nicotinamidase	*Cutibacterium acnes*	193 AA
BCB10818.1	GI:1820239992	nicotinamidase	*Cutibacterium acnes*	193 AA
BBJ75770.1	GI:1755605761	nicotinamidase	*Cutibacterium acnes*	193 AA
BBK84341.1	GI:1681033723	nicotinamidase	*Cutibacterium acnes subsp*	193 AA
CUT97029.1	GI:952556976	nicotinamidase	*Staphylococcus capitis*	184 AA
CUT97845.1	GI:952559501	nicotinamidase	*Staphylococcus capitis*	184 AA
CQD30992.1	GI:910035346	nicotinamidase	*Staphylococcus capitis*	184 AA
CQD29905.1	GI:910030756	nicotinamidase	*Staphylococcus capitis*	184 AA
CQD29714.1	GI:910024066	nicotinamidase	*Staphylococcus capitis*	184 AA
CRN12356.1	GI:871948618	nicotinamidase	*Staphylococcus capitis*	184 AA
CDI71275.1	GI:555595826	nicotinamidase	*Staphylococcus capitis CR01*	184 AA
CEF80765.1	GI:687428060	Uncharacterized isochorismatase family protein PncA	*Staphylococcus aureus*	186 AA
WP_244758597.1	GI:2222898255	bifunctional nicotinamidase/pyrazinamidase, partial	*Staphylococcus aureus*	117 AA
CAJ1322481.1	GI:2565984261	Nicotinamidase-related amidase	*Staphylococcus aureus*	186 AA
CAJ1321780.1	GI:2565983560	Nicotinamidase-related amidase	*Staphylococcus aureus*	186 AA
CAI9426974.1	GI:2513081433	TPA: isochorismatase	*Staphylococcus aureus*	186 AA
CAI9428112.1	GI:2513080255	TPA: isochorismatase	*Staphylococcus aureus*	186 AA
VTS74541.1	GI:1672579366	pyrazinamidase/nicotinamidase (iso-chorismate synthase)	*Staphylococcus aureus*	186 AA
BAX06378.1	GI:1172211922	pyrazinamidase/nicotinamidase-like protein	*Staphylococcus aureus*	186 AA
CRI30366.1	GI:857882610	nicotinamidase	*Staphylococcus aureus*	186 AA
CRI24122.1	GI:857878509	nicotinamidase	*Staphylococcus aureus*	186 AA
CRI26048.1	GI:857861711	nicotinamidase	*Staphylococcus aureus*	186 AA
CRI18746.1	GI:857857772	nicotinamidase	*Staphylococcus aureus*	186 AA
CRI18360.1	GI:857854128	nicotinamidase	*Staphylococcus aureus*	186 AA
CRI13777.1	GI:857850742	nicotinamidase	*Staphylococcus aureus*	186 AA
CRI14483.1	GI:857814294	nicotinamidase	*Staphylococcus aureus*	186 AA
CAG40996.1	GI:49242289	isochorismatase family protein	*Staphylococcus aureus subsp*	186 AA
WP_002457081.1	GI:488387696	MULTISPECIES: isochorismatase family cysteine hydrolase	*Staphylococcus epidermidis*	184 AA

Supplementary table 2

Strain-specific primers of *Cutibacterium acnes*[1], *Cutibacterium granulosum*[2], *Staphylococcus epidermidis*[3], *Staphylococcus capitis*[4], *Corynebacterium simulans*[5], *Staphylococcus aureus*[1], *Malassezia furfur*[5].

Strains	Relative abundance in the Hcm	Primers	Standard curves *Y* (log CFU) / *X* (Ct values)
Cutibacterium acnes (ATCC 6919)	88.7860%	Forward primer 5'-CGAGGAGCAATTTCTGGGAT-3'	y= -4.223x+51.525
		Reverse primer 5'-ATGGATGACTTCGACGATGA-3'	R^2 = 0.9983
Cutibacterium granulosum (CCUG 67158)	6.2192%	Forward primer 5'-ACATGGATCCGGGAGCTTC-3'	y= -3.3978x+43.365
		Reverse primer 5'-ACCCAACATCTCACGACACG-3'	R^2 = 0.9954
Staphylococcus epidermidis (CICC 10398)	4.0755%	Forward primer 5'- CCCCATCTTTTTAAGTGTTTAGGAAT-3′	y= -4.181x+49.339
		Reverse primer 5'- ATCAGTAATGGGAAATAAATCCATATTGA-3′	R^2 = 0.9954
Staphylococcus capitis (BNCC192327)	0.6389%	Forward primer 5'-ATCCAAGTATTTTTCTAATCGCGTATCT-3'	y= -3.562x+44.338
		Reverse primer 5'-GCTGGACTAAAAAGTATAAGAGTATACTGATTA-3'	R^2 = 0.986
Corynebacterium simulans (BNCC352135)	0.1625%	Forward primer 5'-TCAGCGTGACTACGCCCTC-3'	y= -4.812x+55.722
		Reverse primer 5'-RCYTCGCCAGGGCTTCTC-3'	R^2 = 0.9925
Staphylococcus aureus (CICC 26003)	0.1161%	Forward primer 5'-AGGACAATCATGGCAAGCGTAC-3'	y= -3.945x+46.168
		Reverse primer 5'-AACGGACAACATCTAAACTGGC-3'	R^2 = 0.997
Malassezia furfur (ATCC 44344)	0.0018%	Forward primer 5'-CTTTGGGACACACTCTGCAA-3'	y= -4.227x+46.813
		Reverse primer 5'-TCACAAGAACTGCTCCATGC-3'	R^2 = 0.9961

Supplementary table 3

Sebum and moisture measurements of volunteers. Data are expressed as mean ± SD from three (n=3) biologically independent replicates.

Facial skin (Cheeks, nose, forehead, chin)	Sebumeter (μg cm^{-2})	Corneometer (c. n.)	skin type
Healthy 1	41.7 ± 26.5	90.9 ± 3.82	Normal
Healthy 2	43.3 ± 17	80.8 ± 6.84	Normal
Healthy 3	47.7 ± 5.50	44.3 ± 2.62	Normal
Healthy 4	111.5 ± 9.85	62.3 ± 2.33	Oily
Healthy 5	24.7 ± 2.52	9.5 ± 2.78	Dry
Healthy 6	41.7 ± 21.73	88.4 ± 7.59	Normal

Supplementary table 4

The specific method for sample analysis using high-performance liquid chromatography (HPLC) is as follows:

Sample	Instrumentation	Mobile Phase	Gradient Program:	Flow Rate	Column Temperature	UV Detector
α-arbutin & hydroquinone	HPLC (cat# Nexera XR LC-20AD XR, Shimadzu); NUCIFERA C18P 4.6*250 5U (Hanbon)	Water (A)-Methanol (B)	0-11min: 6% B; 11-12min: 6%-45% B; 12-33min: 45%-50% B; 33-38min: 50% B; 38.01-40min: 100% B; 40.01-45min: 6% B;	1.0 mL min^{-1}	20℃	Wavelengths 280nm
niacinamide & nicotinic acid	HPLC (cat# Nexera XR LC-20AD XR, Shimadzu); NUCIFERA C18P 4.6*250 5U (Hanbon)	Methanol 70 mL, Isopropanol 20 mL, Sodium heptanesulfonate 1 g, dissolved and mixed in 910 mL water, pH adjusted to 2.1 ± 0.1 with hydrochloric acid.		1.0 mL min^{-1}	25 ℃	Wavelengths 261nm

References

1. van der Krieken, D. A. et al. An In vitro model for bacterial growth on human stratum corneum. *Acta dermato-venereologica* **96**, 873-879 (2016).
2. Eishi, Y. et al. Quantitative analysis of mycobacterial and propionibacterial DNA in lymph nodes of Japanese and European patients with sarcoidosis. *Journal of clinical microbiology* **40**, 198-204 (2002).
3. Ashraf, A. et al. A novel multiplex PCR assay for simultaneous detection of nine clinically significant bacterial pathogens associated with bovine mastitis. *Molecular and cellular probes* **33**, 57-64 (2017).
4. Wu, Y. Application of real-time PCR technology in the detection of pathogens in sepsis (in Chinese), Xiamen University (2017).
5. Li, Z. A method for identifying three types of rod-shaped bacteria using high-resolution melting curve analysis. CN110512013 (2019).
6. Ilahi, A. et al. Real-Time PCR identification of six *Malassezia* species. *Current microbiology* **74**, 671-677 (2017).